

Coherent quantum transport in disordered systems I: The influence of dephasing on the transport properties and absorption spectra on one-dimensional systems

Jeremy M. Moix, Michael Khasin ‡ and Jianshu Cao

Department of Chemistry, Massachusetts Institute of Technology, 77 Massachusetts Avenue, Cambridge, MA 02139

E-mail: jianshu@mit.edu

Abstract.

Excitonic transport in static disordered one dimensional systems is studied in the presence of thermal fluctuations that are described by the Haken-Strobl-Reineker model. For short times, non-diffusive behavior is observed that can be characterized as the free-particle dynamics in the Anderson localized system. Over longer time scales, the environment-induced dephasing is sufficient to overcome the Anderson localization caused by the disorder and allow for transport to occur which is always seen to be diffusive. In the limiting regimes of weak and strong dephasing quantum master equations are developed, and their respective scaling relations imply the existence of a maximum in the diffusion constant as a function of the dephasing rate that is confirmed numerically. In the weak dephasing regime, it is demonstrated that the diffusion constant is proportional to the square of the localization length which leads to a significant enhancement of the transport rate over the classical prediction. Finally, the influence of noise and disorder on the absorption spectrum is presented and its relationship to the transport properties is discussed.

PACS numbers: 71.35.Cc, 71.35.Aa, 72.20.Ee, 72.10.Di, 05.60.Gg

‡ Current address: NASA Ames Research Center, Moffett Field, California

1. Introduction

Understanding and controlling transport in condensed matter systems is a topic not only of fundamental scientific interest, but also with immediate technological implications. For example, energy transport is one of the key factors determining the efficiency of light harvesting systems, organic photovoltaics, conducting polymers, and J-aggregate thin films [1, 2, 3, 4, 5, 6, 7, 8, 9]. Energy diffusion has also been shown to play a central role in the rate of vibrational relaxation in small molecules and DNA [10, 11, 12, 13]. Despite this seeming diversity, the underlying physical description of these systems is surprisingly similar. In each case, the transport occurs across a disordered energy landscape that is modulated by thermal fluctuations from the surrounding environment. The relative importance of the strength of the disorder and the thermal fluctuations to the electronic coupling may however vary greatly from system to system. For example, energy transport in J-aggregates are generally characterized by relatively weak disorder and exciton-phonon coupling, while in natural light harvesting systems all of the relevant energy scales are of comparable magnitude [8, 14]. This subtle difference in the parameter regimes leads to markedly different physical behavior in these two systems.

In general the transport properties are relatively well-understood in the presence of either noise or disorder, but less is known when both are present simultaneously. For example, in the case of static, one- or two-dimensional systems, Anderson localization occurs for any finite amount of disorder leading to a complete lack of transport in the long-time limit [15, 16, 17, 18, 19, 20]. In the alternative setting of a system subjected to noise but not disorder, the transport is also –at least qualitatively– understood. In particular, the Haken-Strobl-Reineker (HSR) model, which describes a quantum system coupled to a high temperature Markovian bath, is exactly solvable [21, 22, 23, 24, 25]. The transport qualitatively behaves like that of a classical Brownian process, with an initial period of ballistic expansion before transitioning to diffusive transport at long times.

The situation is more complicated when a disordered system is coupled to an environment. Thermal excitation from low-lying localized states into more extended higher energy states can be sufficient to overcome the Anderson localization and allow for transport to occur at long times [26]. In particular, Mott’s theory of variable range hopping has been quite successful in describing the behavior of the low temperature conductivity of disordered systems [27]. More recently, Logan and Wolynes have analyzed the role of dephasing in topologically disordered systems and provided approximate scaling relations for the transport [28, 29, 30]. Their analysis and preliminary numerical results suggest that the diffusion coefficient should display a non-monotonic dependence on the system-bath coupling strength [31]. However, a general description of the transport valid for all temperatures is still lacking. Alternatively, it has also been shown that an external driving force containing a few independent frequency components is equally sufficient to restore diffusive motion in the long time

limit to an otherwise localized system [32]. In summary, while any finite amount of disorder leads to a lack of diffusion in one or two-dimensional systems, adding a source of dephasing can be sufficient to allow for transport to occur by destroying the phase coherence responsible for Anderson localization.

Here, we carry out numerically exact calculations of infinite one-dimensional disordered systems over the entire regime of dephasing within the HSR model. In section 2.1 quantum master equations are derived for the time evolution of the density matrix in the limiting regimes of weak and strong dephasing. These results allow for analytical estimates of the diffusion constant and provide an intuitive physical description of the underlying dynamics. For large dephasing, it is well known that any coherences created during the evolution are quickly destroyed and the diffusion proceeds by way of classical hopping between sites [33, 34]. In the opposite regime of weak dephasing, the exact eigenstates of the system are accurately approximated by those of the disordered system Hamiltonian, and coherent quantum transport proceeds via hopping through the eigenstates. This is the regime of phonon-assisted hopping discussed in the early studies of the conductivity of disordered solids [35]. These analytical arguments coupled with the exact numerical calculations lead to several interesting features in the exciton dynamics:

- The strong and weak dephasing master equations allow one to extract the respective scaling behavior of the transport properties which suggests the existence of a maximum in the diffusion coefficient as a function of the dephasing rate. This prediction is confirmed numerically in section 3. It should be mentioned that similar scaling studies have been carried out in the context of noise-assisted transport in excitonic systems [36, 37]. There, however, the focus is mostly on the optimal energy transfer time in finite systems, and the results are largely consistent with a purely classical analysis [38]. In the present case there is a genuine and unambiguous quantum aspect to the transport.
- In the weak dephasing regime, it is demonstrated that the diffusion constant is proportional to the Anderson localization length of the disordered system Hamiltonian. This implies that for systems weakly coupled to the environment, the coherent nature of the transport leads to a diffusion constant that is enhanced by a factor of the localization length as compared to the classical prediction.
- The third primary result of this work is related to the initial, non-diffusive nature of the transport. Over a timescale on the order of the inverse dephasing rate the dynamics are ballistic until the Anderson localization length of the system is reached [39]. The corresponding population probability distribution during this period is exponential reflecting the exponential localization of all wavefunctions. At longer times, the influence of the dephasing becomes more important leading to diffusive motion with a characteristic Gaussian probability distribution. As a result, the mean-squared displacement can be described as a combination of the short-time ballistic transport in the localized system and the long-time diffusive

transport.

- Finally we present results on the influence of disorder and dephasing on the absorption spectra. For many materials, such as photovoltaics, the organic semiconductor must possess not only favorable energy transport characteristics, but also a broad absorption spectrum in order to capture as much solar energy as possible. It is demonstrated that while reducing the disorder leads to enhanced transport, it also leads to a narrower absorption line shape which is not optimal in this case. Therefore, we present a detailed study of the effects of dephasing and disorder on the absorption lineshape.

The paper is concluded in section 4 where the practical implications of these findings are discussed. For systems such as conducting polymers where the transport properties are the key factor governing the device performance, then one should primarily seek to reduce the amount of static disorder present in the sample. Recent experimental results on the conductivity of conducting polymers and light harvesting systems are discussed in this context.

2. Model Systems and Scaling Analysis

The HSR model describes quantum transport in the presence of a classical Markovian environment [21]. At equilibrium all sites are equally populated, and as such, the results presented here are strictly valid only in the high temperature limit. Nevertheless, the model is capable of capturing many of the essential physical features of real systems.

In the wavefunction description of the HSR model, the thermal environment is modeled as a white noise term that modulates the site energies of the system Hamiltonian which is described by the stochastic Schrödinger equation,

$$i \frac{d}{dt} |\psi\rangle = H_s |\psi\rangle + \sum_n^N F_n(t) V_n |\psi\rangle, \quad (1)$$

where $V_n = |n\rangle \langle n|$ characterizes the system-bath coupling in the local basis, and the sum extends over all $N \rightarrow \infty$ sites of the system. The time-dependent factors, $F_n(t)$, are zero-mean Gaussian stochastic (Wiener) processes with $\langle F_n(t) \rangle = 0$, and the autocorrelation, $\langle F_n(t) F_m(t') \rangle = \Gamma \delta_{nm} \delta(t - t')$. In this context, the dephasing rate, Γ , determines the magnitude of the fluctuations. In order to recover the exact time evolution, the wavefunctions must be ensemble averaged over realizations of the noise.

Alternatively, due to the simple noise characteristics of the bath the averaging over the environmental fluctuations may be performed analytically. This procedure leads to an equivalent deterministic equation of motion for the density matrix,

$$\dot{\rho}(t) = -i [H_s, \rho] - \frac{\Gamma}{2} \sum_n [V_n, [V_n, \rho]]. \quad (2)$$

From a numerical standpoint, the density matrix approach is more efficient for small systems, while the stochastic implementation becomes essential for larger systems.

The bare system is characterized by a one-dimensional tight-binding, Anderson Hamiltonian

$$H_s = \sum_n \epsilon_n c_n^\dagger c_n + J \left(c_n^\dagger c_{n+1} + c_{n+1}^\dagger c_n \right), \quad (3)$$

where J denotes the electronic coupling strength. Static disorder is introduced into the system Hamiltonian by taking the site energies, ϵ_n , as independent, identically-distributed Gaussian random variables characterized by the variance, $\sigma^2 = (\epsilon_n - \overline{\epsilon_n})^2$. Throughout, the averages over the static disorder are denoted by the overline while the quantities denoted by angle brackets characterize the quantum-mechanical average over the environment.

The HSR model for the disordered system is completely characterized by only three parameters: the electronic coupling between sites, J , the variance of the static disorder, σ^2 , and the dephasing rate, Γ . The electronic coupling J is used to set the energy scale throughout, which leaves only two independent dimensionless quantities, Γ/J and σ/J . In our simulations, the HSR is always seen to lead to diffusion at long times and we extract the diffusion constant, D , from the limiting behavior of the mean-squared displacement (MSD),

$$2Dt = \lim_{t \rightarrow \infty} \overline{\langle R^2(t) \rangle}. \quad (4)$$

The mean-squared displacement is calculated from,

$$\langle R(t)^2 \rangle = \sum_n n^2 \rho_{nn}(t), \quad (5)$$

with the origin conveniently chosen such that the first moment is zero.

It is not immediately obvious that the transport should always be diffusive, particularly in the weak dephasing regime where the effects of both Anderson localization and quantum coherence are prevalent. In the classical limit and in the disorder-free case, it can be shown analytically that the transport is always diffusive in the long time limit. But outside of these two regimes there is no known proof (at least to our knowledge) that the MSD is guaranteed to increase linearly with time in the steady state. However, all of our numerical simulations as well as those of similar earlier analytical and numerical results suggest that the transport is indeed diffusive [26, 40, 31].

In addition to the transport properties, we also compute the linear absorption spectrum from the dipole autocorrelation function [41],

$$A(\omega) \propto \text{Re} \int_0^\infty dt e^{i\omega t} \overline{\langle \mu(t) \mu(0) \rangle}, \quad (6)$$

where the dipole moment operator is given by, $\mu = \sum_n \mu_n (|n\rangle\langle 0| + |0\rangle\langle n|)$. Since all of the molecules in the system are assumed identical, we take the magnitude of the individual dipole moments equal to the constant value $\mu_n = \mu_0$.

In the numerical simulations presented below the dynamics were performed in one-dimensional chains of up to 500 sites and averaged over 500 to 1000 independent realizations of the static disorder. The transient short-time effects of the transport

properties decay on the order of J/Γ so that the dynamics are required for at least an order of magnitude longer in order to obtain a reliable estimate of the diffusion coefficient.

2.1. Limiting behavior of the transport properties

2.1.1. Homogeneous systems When the disorder is absent ($\sigma = 0$), the HSR model is analytically solvable. In this case the MSD is given by [21, 22, 42],

$$\langle R(t)^2 \rangle_{\sigma=0} = \frac{4J^2}{\Gamma} \left[t - \frac{1}{\Gamma} (1 - e^{-\Gamma t}) \right], \quad (7)$$

which is equivalent to that of a Brownian particle. For a time of the order of Γ^{-1} , the transport displays free-particle, ballistic behavior ($\langle R(t)^2 \rangle \propto t^2$) which transitions to diffusive motion at long times with the diffusion coefficient,

$$D_{\text{hom}} = 2J^2/\Gamma. \quad (8)$$

It is clearly seen that (8) diverges at small dephasing. However, if $\Gamma = 0$ exactly, then any amount of disorder will lead to Anderson localization and no diffusion. In this interesting regime of vanishing dephasing but finite disorder the dynamics are highly coherent and display a sensitive dependence on the model parameters. This region will be explored in depth in the numerical simulations presented in section 3.

2.1.2. Strong damping regime: hopping rate In the presence of both dephasing and disorder, analytic expressions for the MSD valid for the entire parameter regime are no longer available. However, if the dephasing rate is sufficiently large such that $\Gamma/J \gg 1$ then any coherences created during the course of the time evolution are quickly destroyed. In this case, (2) reduces to a model of classical hopping between neighboring sites [33]. As has been shown previously, averaging the hopping rates over the disorder distribution leads to the diffusion coefficient [43, 33, 34],

$$D_{\text{hop}} = \frac{2J^2\Gamma}{\Gamma^2 + \sigma^2}. \quad (9)$$

Notice that (9) displays a non-monotonic dependence on Γ , and in particular, optimal transport when $\Gamma_{\text{opt}} = \sigma$. For large dephasing, (8) is recovered, and reduces to $D_{\text{hop}} \approx 2\Gamma J^2/\sigma^2$ at small dephasing.

The linear increase in the diffusion constant for $\Gamma/J \ll 1$ has been previously discussed in the context of noise-assisted transport [33, 34]. However, (9) is applicable only when the classical hopping description is appropriate. In the weak dephasing regime the dynamics are highly coherent so the prefactor predicted by the classical hopping description of the dynamics can not be correct. As the dephasing decreases, the exact eigenstates of the total system rotate from the local basis into the exciton basis, and the wavefunctions will delocalize over coherent domains. The size of these domains is on the order of the Anderson localization length, which, in turn, is governed by the disorder strength [8, 19]. The short-time dynamics of an initial localized excitation in the chain

will be characterized by a rapid expansion filling one of these localized domains. Over a longer timescale (of the order of J/Γ) the dephasing will allow for the collective hopping of the delocalized states among the various localization segments. These qualitative arguments are formalized in the following subsection through the development of a weak-coupling master equation.

2.1.3. Weak damping regime: coherent transport In the weak dephasing regime, an accurate description of the exciton dynamics may be obtained from the Redfield equation. Since the system is disordered and the diffusion constant depends only on the long-time dynamics, the secular and Markov approximations can be employed without a significant loss of accuracy. In this case, the exciton populations are governed by the master equation,

$$\dot{\rho}_{\kappa\kappa}(t) = \sum_{\lambda \neq \kappa} W_{\kappa\lambda} \rho_{\lambda\lambda}(t) - \sum_{\lambda \neq \kappa} W_{\lambda\kappa} \rho_{\kappa\kappa}(t), \quad (10)$$

where the rates,

$$W_{\kappa\lambda} = W_{\lambda\kappa} = \Gamma \sum_n |\langle \kappa | n \rangle \langle n | \lambda \rangle|^2. \quad (11)$$

The Greek labels here denote eigenstates of the static disordered system Hamiltonian (exciton states). The equivalence of the forward and backward rates is a consequence of the high temperature nature of the thermal environment. In the secular approximation, the coherences are decoupled from the populations and their time evolution can be determined analytically as, $\rho_{\kappa\lambda}(t) = e^{-(i\omega_{\kappa\lambda} + \Gamma - W_{\kappa\lambda})t} \rho_{\kappa\lambda}(0)$, where $\omega_{\kappa\lambda}$ is the difference in eigenenergies between states κ and λ .

Equation (10) is a Markovian master equation that describes hopping through the eigenstates of the disordered system. The rates –and hence the diffusion constant– increase linearly with Γ as with the weak dephasing limit of the classical hopping result in (9). However, here there is an important difference in that the Redfield rates are now correctly weighted by the eigenstate overlaps. The classical hopping rates capture the correct dephasing dependence of the diffusion constant, but incorrectly describe the disorder dependence of the prefactor. As will be shown below, this difference is substantial in many physically relevant situations.

The eigenstate overlaps in the Redfield rates are determined solely by the disordered system Hamiltonian. Therefore, they depend only on the ratio of σ/J . In order to understand this disorder dependence consider, for example, the rate element $W_{\kappa\lambda}$. Due to the static disorder, the eigenstate λ will be localized at a position n_λ in the chain with a spatial extent, ξ_λ , and similarly for state κ . On average, the spatial extent of κ and λ is determined by the Anderson localization length, ξ . As a result, the rate $W_{\kappa\lambda}$ can be appreciable only if the states κ and λ are located at position in the chain within an Anderson localization length of one another. That is, $|n_\kappa - n_\lambda| \lesssim \xi$. One sees that the fundamental length scale governing the magnitude of the rates in the Redfield description is given by the spatial extent of the wavefunctions, i.e., the Anderson localization length.

Hence, on scaling grounds we expect the diffusion constant to have the following form,

$$D_{\text{coh}} = \Gamma \xi^2 , \quad (12)$$

where the factor, ξ , is directly proportional to the Anderson localization length. As in the large dephasing limit, the diffusion in the weak dephasing regime may also be interpreted as a hopping process except that here the fundamental step size is determined by the localization length. The mean-field theory results of Logan and Wolynes have also arrived at a similar conclusion [28, 31]. Their approach indicates that the localization length appearing in (12) is, in fact, simply the inverse participation ratio. This result is consistent with our numerical results presented below, although our preliminary calculations in two-dimensional systems indicate that this result is only correct up to a scaling constant.

2.2. Localization Length

Due to the intense interest in the problem of Anderson localization, accurate scaling relations are known for the localization length in disordered systems [17, 40]. In one dimension systems, the localization length is directly proportional to the mean-free path, $\xi \propto J^2/\sigma^2$. In two dimensions the localization length is exponentially larger than it is in one dimension, and metallic transport appears at a critical value of the disorder strength in three-dimensional systems [40]. Transport in these systems will be discussing in a future work, but is beyond the scope of the present paper. In order to fix the proportionality, we will use the inverse participation ratio (IPR) as a proxy for the localization length in the disordered chain, as suggested by Logan and Wolynes. The IPR is defined for a particular eigenstate, κ , as

$$\xi_{\kappa} = \left(\sum_n |\langle n | \kappa \rangle|^4 \right)^{-1} . \quad (13)$$

Figure 1 presents the scaling of the IPR as a function of the disorder computed by direct diagonalization of the disordered system Hamiltonian. Due to the high temperature approximation inherent to the HSR model, all of the eigenstates are equally capable of contributing to the transport. Therefore the IPR presented in figure 1, $\langle \xi \rangle$, is averaged over all eigenstates, which reproduce the known functional dependence of the localization length.

2.3. Implications of the scaling limits

Based on the limiting behavior of the transport deduced above from the master equations, several intriguing physical aspects of the transport become apparent. For example, in the weak dephasing regime the quantum coherent nature of the transport can lead to a considerable enhancement of the diffusion constant compared with the classical

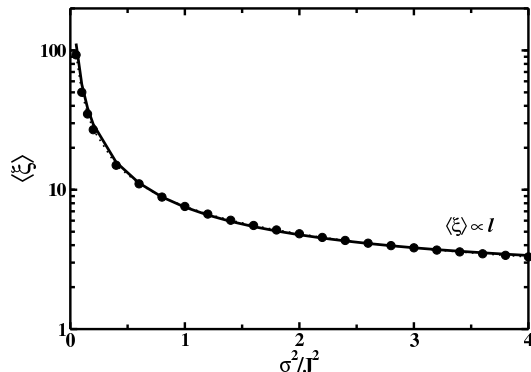


Figure 1. The scaling of the inverse participation ratio as a function of the disorder strength computed in systems containing up to 4900 sites. The symbols represent the exact numerical results and the solid lines depict the fit to the functional form predicted from the scaling theory of Anderson localization. Specifically, the IPR is fit to the line $\xi \approx 5.5l$, with the mean free path, $l = J^2/\sigma^2$.

estimate. For $\Gamma/J \ll 1$, this “quantum speedup” can be determined analytically and is given by

$$D_{\text{coh}}/D_{\text{hop}} = \frac{\xi^2}{2l} \propto \xi, \quad (14)$$

which can be quite substantial for reasonable values of the systems parameters, as seen from figure 1. The enhancement is proportional to the localization length as a result of the enhanced step size of the hopping process in the weak dephasing regime.

Secondly, in the weak dephasing regime the transport increases linearly with Γ (10) while for strong dephasing the diffusion decreases as Γ^{-1} (9), which implies that the diffusion constant should be maximal at intermediate values of the dephasing. As mentioned above, (9) also predicts an optimal diffusion constant at $\Gamma_{\text{opt}} = \sigma$. However, this estimate is only correct for very large disorder and becomes increasingly worse as the system becomes more coherent, as will be demonstrated in the numerical results presented in the next section. An improved estimate for the optimal dephasing rate may be obtained by equating the proper weak dephasing limit of (12) with the large dephasing result in (8). This leads to the improved estimate,

$$\Gamma_{\text{max}} = \sqrt{2}J/\xi, \quad (15)$$

which will be shown to be substantially more accurate than the prediction provided by (9).

The existence of a maximum in the diffusion coefficient is a result of the interplay between the Anderson localization due to static disorder and thermal localization originating from the environment [44]. The optimum occurs in the regime where the exact eigenstates of the total system transition between the local site basis and the exciton basis. For example, in an initially Anderson localized system increasing

the dephasing rate enhances the transport, but it also serves to further localize the wavefunctions which reduces the hopping length. It is this competition that is responsible for the non-monotonic behavior of the transport and is generic to many systems. Similar arguments for the non-monotonic behavior of the transport have been presented in [36] as well as a similar estimate for the optimal dephasing rate as (15).

3. Numerical Results

3.1. Diffusion Coefficients

The diffusion coefficients calculated from the above approaches are shown in figure 2(a) as a function of the dephasing rate. In agreement with the discussions of the previous section, When $\Gamma/J \gg 1$ the exact numerical results agree with the prediction of the classical hopping model in (9) (dotted lines). At even larger values of the dephasing, the diffusion constant becomes independent of the disorder and the results coincide with estimate of (8) for the homogeneous chain (dot-dashed line). However, one notices that as the disorder decreases and the dynamics become more coherent the classical hopping approximation quickly deteriorates in predicting both the magnitude of the diffusion constant as well as the location of the maximum. For sufficiently weak dephasing, $\Gamma/J \ll 1$, the exact numerical results are in agreement with the numerical calculations of the Redfield equation (square symbols in figure 2(a)). The latter are seen to be in excellent agreement with the scaling relation of (12) (dashed lines), with the localization length, ξ , determined from the IPR calculations in figure 1.

In order to further explore the role of coherence in the dynamics, figure 2(b) displays the ratio of the exact numerical diffusion coefficients shown in figure 2(a) to the classical hopping prediction, D/D_{hop} . For $\Gamma/J > 1$, the exact and classical hopping results are approximately equivalent since an coherence generated during the time evolution of the populations are quickly destroyed by the strong dephasing. However, as the dephasing decreases the dynamics become more coherent leading to a significant increase in the ratio of D/D_{hop} . In the asymptotic regime where $\Gamma/J \ll 1$, the exact numerical results approach the limiting values given in (14) (cross symbols) which are determined only by the Anderson localization length of the static system Hamiltonian. As discussed above, the transition from coherent dynamics in the weak dephasing regime to the classical hopping dynamics is due to the fact that in addition to the static disorder, the thermal environment can also serve to localize the system. That is, the true localization length is a function of both σ and Γ . In the limit $\Gamma = 0$, the localization is entirely due to Anderson localization whereas for $\Gamma/J \gg 1$ the localization is largely due to the dephasing. Indeed, the results in figure 2(b) may be interpreted as a measure of the true localization length in the system.

As mentioned, the dephasing can play an equally important role to the static disorder in localizing the system. It would be highly desirable to be able to quantify the localization that occurs due to the dephasing. This is generally affected through

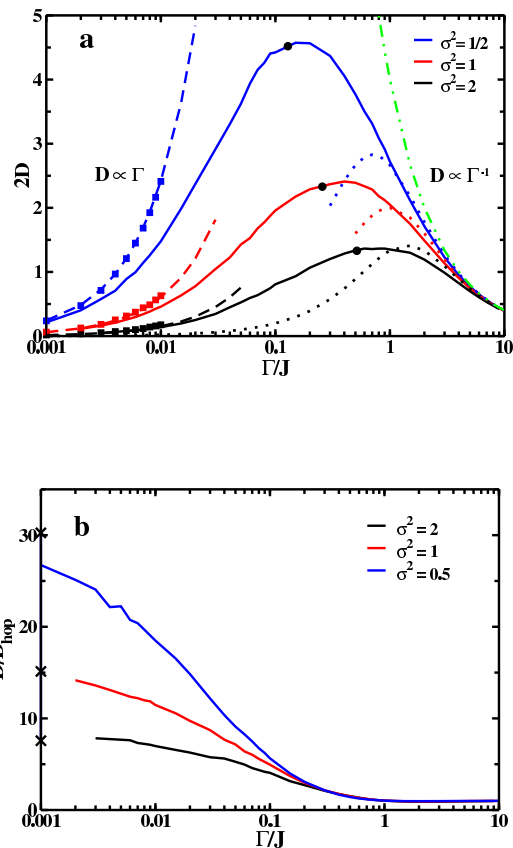


Figure 2. (a) Diffusion constants calculated as a function of the dephasing rate. The solid blue, red, and black lines are the exact numerical simulations of (2) for $\sigma^2/J^2 = 1/2, 1,$ and $2,$ respectively. The filled squares at small dephasing display the results of the secular Redfield equation and the dashed lines provide the corresponding analytic results of (12). At large dephasing, the dotted lines depict the classical hopping estimates of (9) and the dot-dashed line is the exact result of (8) for $\sigma^2 = 0.$ The solid black dots indicate the estimate for location of the optimal dephasing rate provided in (15). (b) The ratio of the numerically exact diffusion constant in (a) to the classical hopping result of (9). The cross-symbols on the ordinate indicate the limiting values given by $D_{\text{coh}}/D_{\text{hop}}$ in (14).

computations of the equilibrium reduced density matrix [44]. However, the equilibrium state of systems described by the HSR model is somewhat trivial due to the infinite temperature bath. Each site is equally populated and the system is completely localized in the site basis. Based upon this observation one would expect the classical hopping description to always be applicable, which is clearly not the case as shown above. The failure of this approach lies in the realization that there is an inherent difference between the equilibrium state in a large, but finite chain and the nonequilibrium steady-state of an infinite chain where the populations are continuously evolving. If one considers the distribution of populations, then tails of the distribution represent the sites where

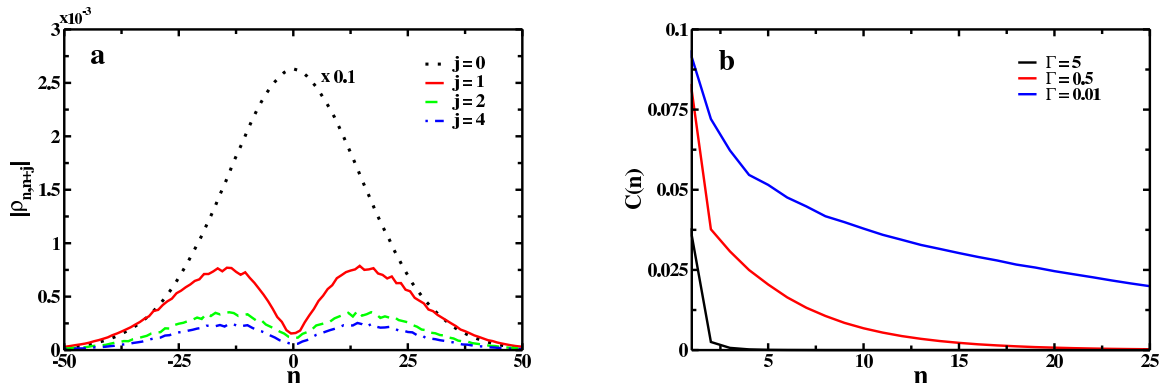


Figure 3. (a) The absolute value of the density matrix elements computed in the steady state for the parameters $\Gamma/J = 0.5$ and $\sigma/J = 1$. The various values of j represent the j -th superdiagonal of the density matrix. The populations ($j = 0$) have been scaled by a factor of 0.1 in order to reside on the same scale as the coherences ($j = 1, 2$, and 4). (b) The mean coherences present in the steady state density matrix as determined from (16) with $\sigma/J = 1$.

the population is spreading to new sites in the chain. In this region coherences are constantly being created and destroyed. The spatial extent of these coherences also reaches a steady state, and it is this coherence length that is responsible for the deviations from the classical hopping result. The interior of the probability distribution, however, equilibrates. In order to demonstrate this point more clearly, figure 3(a) displays slices through a snapshot of the steady-state density matrix taken in the regime where an accurate estimate of the diffusion coefficient is possible. One sees that the populations (dotted line) display the Gaussian profile expected of a diffusion process. The coherences are substantial only in the tails of the population distribution, while the interior thermalizes and becomes diagonal in the local basis. In an infinite chain, this process continues indefinitely. At longer times, the coherences in the center of the chain will be further depleted while new coherences will be created in the extremities as the populations evolve.

In order to quantify the role of dephasing in localizing the system, it is necessary to characterize the amount of coherence present in the density matrix in the diffusive, steady-state regime. Unfortunately, as seen above there is no way to unambiguously determine this coherence length. As a simple qualitative measure we will use the metric,

$$C(n) = \sum_i |\overline{\rho_{i,i+n}}|, \quad (16)$$

computed from the steady-state density matrix in the long-time limit where a reliable estimate of the diffusion constant is possible. The correlation function $C(n)$ is simply the sum of the individual superdiagonals of the density matrix displayed in figure 3(a). As can be seen in figure 3(b), both the magnitude and spatial extent of $C(n)$ clearly depend

on the dephasing. For $\Gamma/J \gg 1$ the dephasing may completely localize the system in the site basis regardless of the disorder. Unsurprisingly, in this regime the classical hopping approximation to the transport is highly accurate as seen above in figure 2(a). In the opposite regime, the dephasing has less influence on localizing the system, and the extent of the wavefunctions is predominantly determined by the Anderson localization due to static disorder. Optimal diffusion occurs in the intermediate regime, where both the noise and disorder play a role in the localization of the wavefunctions.

3.1.1. Improved diffusion estimates It is interesting to explore the question if the thermal localization can be used to extend the regime of validity of the scaling behavior obtained from the Redfield equation in (12). To this end, we propose a simple ansatz for a dephasing-dependent correction to localization length, $\tilde{\xi}(\Gamma) = f(\Gamma)\xi$, with $0 \leq f(\Gamma) \leq 1$, which leads to the corresponding diffusion constant,

$$D_{\text{coh},\Gamma} = \Gamma \tilde{\xi}(\Gamma)^2 . \quad (17)$$

The behavior of $f(\Gamma)$ can be determined by noting that for disordered systems, $C(n)$ falls off exponentially for large n regardless of the dephasing. That is, $C(n) \sim e^{-n/L_\Gamma}$ with the characteristic length scale denoted by L_Γ . Therefore, it is possible to define the correction factor $f(\Gamma) = L_{\Gamma=0}/L_\Gamma$, where $L_{\Gamma=0}$ is obtained in the dephasing-free, Anderson localization limit. From the steady-state density matrix, we compute $C(n)$ and then fit the exponential decay at large n to obtain $f(\Gamma)$. The results of this procedure for computing the dephasing-corrected diffusion coefficient are displayed in figure 4(a). For small dephasing rates, the modified diffusion coefficient corrects the overestimation of (12) and even predicts the turnover seen in the exact results. The agreement with the exact numerical results is of course only qualitative, but one could easily devise a more sophisticated approach by demanding, for example, that (17) also reproduces the correct large dephasing limit. However the main point of this argument is to provide and intuitive illustration of the influence of dephasing and disorder on the transport dynamics discussed above.

While perhaps useful, it should be noted that this procedure for correcting the weak dephasing scaling limit is not a constructive approach. That is, computing the dephasing-induced localization length requires the steady-state density matrix, which alone is sufficient to determine the exact diffusion constant. However, a more direct and accurate approach to characterize the thermal localization length could prove a useful route to a uniform approximation of the diffusion constant.

Although the above discussion provides a physically motivated uniform approximating to the diffusion coefficient, a simple alternative has been proposed by Thouless and Kirkpatrick [26]. They cleverly suggest to use an interpolating formula,

$$D_{\text{interp}} \approx \left[\left(\frac{2J^2}{\Gamma + \sigma/2} \right)^{-1/2} + (\Gamma\xi^2)^{-1/2} \right]^{-2} , \quad (18)$$

which reduces to the correct limits in both the strong and weak dephasing regimes, and reasonably bridges the intermediate region. Figure 4(b) displays the exact numerical

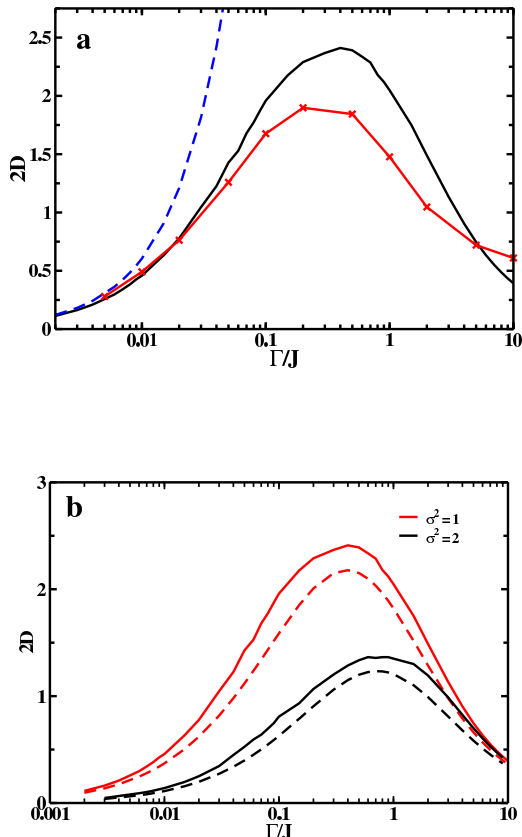


Figure 4. (b) The exact numerical results for the diffusion constant for $\sigma/J = 1$ reproduced from figure 2(a) along with the weak dephasing result from (12) (blue dashed line). The solid (red) line with cross symbols denote the improved scaling relation of (17). (b) The exact numerical results for the diffusions coefficients from figure 2(a) (solid lines) computed at $\sigma^2/J^2 = 1$ (red) and 2 (black). The corresponding approximate results of (18) are displayed as the respective dashed lines.

results for the diffusion constant computed previously in figure 2(a) with $\sigma^2/J^2 = 1$ and 2 (solid lines), along with the corresponding approximation from (18) (dashed lines). This approach performs well in one-dimensional systems discussed here, although in our preliminary studies of two-dimensional systems this simple interpolation appears to be less satisfactory.

3.2. Non-diffusive dynamics

While the behavior of the diffusion coefficient is interesting, it is also useful to understand the dynamical properties of noisy, disordered systems. In figure 5(a) the initial MSD is shown for short times ($\Gamma t = 1$). For $\sigma = 0$ but finite dephasing, the exact MSD is given by (7). Over the time scale shown, this result (dotted line) leads to purely ballistic, free-particle motion, and substantially overestimates the transport. For $\Gamma = 0$, but

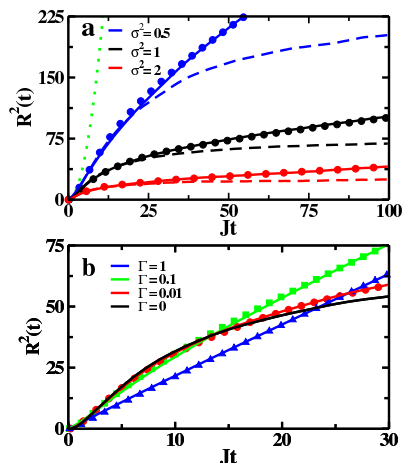


Figure 5. In (a), the dashed blue, red, and black lines depict the MSD for $\Gamma = 0$, and $\sigma^2 = 1/2, 1$, and 2 . This case is exactly the bounded dynamics due to Anderson localization and provides a lower bound to the transport. The solid lines depict the corresponding results with $\Gamma = 0.01$. The green dotted line is the exact result of (7) for $\sigma = 0$. This case represents free diffusion in the homogeneous chain and defines the upper bound to the transport rate. Figure (b) displays the MSD at very short time for $\sigma^2 = 1$. The black, red, green, and blue lines correspond to dephasing rates of $\Gamma = 0, 0.01, 0.1$, and 1 . The symbols are exact numerical results and the solid lines are the fits to (19) with $\eta = 0.84, 0.2$ and, 0.04 .

finite disorder (dashed lines), the motion is again described by that of a free particle, although now in a disordered environment. In this case, the dynamics are also ballistic, but only until the localization length is reached at which point the transport stops. This behavior is similar to that of a particle in a box where the size of the box is determined by the Anderson localization length. The limit of $\Gamma = 0$ provides a lower bound to the transport whereas the homogeneous chain limit of $\sigma = 0$ provides an upper bound.

The solid lines in figure 5(a) display the results for the corresponding disordered system with the addition of weak dephasing ($\Gamma/J = 0.01$). As can be seen, the coupling to the high-temperature environment allows the wavepacket to overcome the localization barriers, eventually leading to diffusion. Additionally, for short times the MSD essentially mirrors that of the corresponding $\Gamma = 0$ results. That is, for weak dephasing, the initial dynamics can be qualitatively described by those of a free particle in a disordered chain. Consistent with the arguments that led to the estimate for the diffusion constant in (12), there are two time scales present in the weak dephasing limit. The fast time scale is described by the (ballistic) free particle expansion in the Anderson localized chain. Over a longer time scale, of order Γ^{-1} , the diffusive transport becomes dominant due to role of the dephasing. It is interesting to note the possibility that for sufficiently small dephasing the non-diffusive motion could persist over a timescale such that it is comparable with exciton dissociation or recombination.

In figure 5(b), the role of the dephasing rate on the short-time, free-particle behavior is shown. For smaller dephasing rates, the dynamics are essentially identical to the $\Gamma = 0$

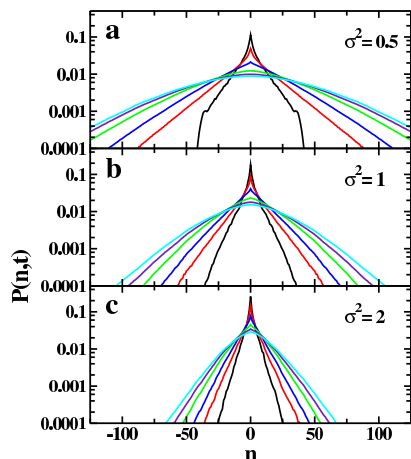


Figure 6. The probability distributions at times $\Gamma t = 0.2$ (black), 2 (red), 5 (blue), 10 (green), 15 (purple) and 20 (cyan) calculated with $\Gamma = 0.01$. Panels (a), (b), and (c) correspond to $\sigma^2 = 0.5, 1$, and 2 , respectively.

result over the time scale shown. At very short-times, the free particle motion ($\Gamma = 0$) provides an upper bound to the rate of spreading. As the dephasing rate increases, the departure of the respective MSD from the $\Gamma = 0$ result occurs sooner. Similar transient localization effects have been observed in semiclassical simulations of the transport of organic semiconductors and quasicrystals [39, 45]. Based on these observations, one can approximate the MSD at any dephasing rate as a linear combination of the $\Gamma = 0$, free-particle result and the long-time linear diffusion,

$$\overline{\langle R(t)^2 \rangle} \approx 2dDt + \eta(\sigma, \Gamma) \overline{\langle R(t)^2 \rangle}_{\Gamma=0}, \quad (19)$$

where the parameter, $0 \leq \eta \leq 1$. As the dephasing rate increases, the prefactor, η , decreases. The symbols in figure 5(b) display the exact numerical results and the solid lines are the corresponding fits to (19). This fit becomes quantitative in the small dephasing regime where $\eta \sim 1$. In the general case, (19) accurately describes the dynamics at both short and long times, with a small discrepancy in the intermediate regime.

Figure 6 displays the average probability distributions of the site populations at $\Gamma/J = 0.01$ and $\sigma^2/J^2 = 0.5$ (a), 1 (b), and 2 (c) for an initial excitation located at a single site in the center of the disordered chain. In all three cases the tails of the distribution functions appear exponential at short times and transition to Gaussian at long times. In driven disordered systems [32], it was proposed that the probability distribution at any fixed time can be fit as $P(n) \propto e^{-\phi|n|^\gamma}$, where the scaling exponent, $1 \leq \gamma \leq 2$ and $\phi \geq 0$. Physically, this expression arises from the observation that at short times, all of the eigenstates are exponentially localized, which leads to a corresponding exponential probability distribution for the populations ($\gamma = 1$). At long times, the motion is diffusive implying a Gaussian probability distribution with $\gamma = 2$. For the HSR model, this picture is only qualitatively correct. It clearly can not capture the

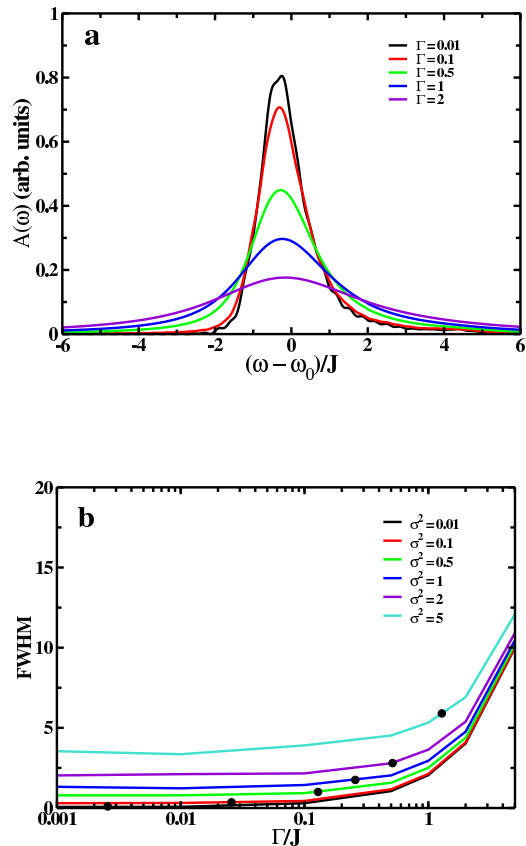


Figure 7. (a) Absorption spectra of a disordered linear chain calculated at $\sigma/J = 1$. (b) Full width at half maximum as a function of the dephasing rate for various values of the disorder. The solid dots display the value of the dephasing for which the transport is maximized from (15).

persistent sharp peak at the origin that arises from the initial excitation or the wavefront of the initial ballistic spreading seen at $\Gamma t = 0.2$ for $\sigma^2 = 0.5$.

3.3. Absorption spectra

From the above results, it is clear that the diffusion coefficient is strongly influenced by the amount of disorder present in the system. While reducing the amount of disorder will improve the transport properties, this is often not the only material characteristic that is important for the overall device performance. For instance, in the case of organic photovoltaics the organic semiconductor should ideally possess not only a high mobility but also a broad absorption spectrum in order to capture the largest portion of the solar spectrum. Therefore in order to understand the interplay of the transport properties and absorption characteristics, figure 7(a) displays the effect of the dephasing on the absorption spectrum computed from (6) with $\sigma^2/J^2 = 1$. In contrast to the

diffusion coefficient, the dipole-dipole correlation function decays rapidly to zero on a timescale on the order of Γ^{-1} . That is, the absorption spectrum is determined by the short-time, non-diffusive dynamics of the wavepacket (cf. figure 5) rather than the long-time linear behavior of the MSD. In figure 7(a), the spectra computed at $\Gamma/J = 0.01$ is indistinguishable from the spectrum calculated with disorder only (see (A.1)) and is governed only by inhomogeneous broadening mechanisms. In this case, the lineshape displays the characteristic asymmetric profile commonly observed in the low-temperature spectra of excitonic systems –a Gaussian profile for $\omega < \omega_0$ and Lorentzian lineshape for $\omega > \omega_0$ [46, 47]. Only at very large disorder, $\sigma/J \gg 1$, does the inhomogeneously broadened spectrum become purely Gaussian. As the dephasing is increased, the spectra are broadened into a Lorentzian lineshape indicative of systems dominated by homogeneous broadening. A detailed discussion of the absorption spectra and the associated lineshape is provided in Appendix A.

In order to investigate the relationship between spectral properties and transport properties in more detail, it is useful to analyze the full width at half maximum (FWHM) of the absorption spectrum as a function of the dephasing rate and disorder as shown in figure 7(b). As discussed previously at small dephasing, the linewidth is determined solely by inhomogeneous broadening mechanisms which leads to the plateau in the FWHM for $\Gamma/J \ll 1$. In the opposite regime of large dephasing, the spectra are purely Lorentzian with a linewidth that scales linearly with the dephasing rate as discussed in Appendix A. The solid dots in figure 7(b) denote the value of the dephasing for which the transport is maximal as predicted from the scaling relation of (15). At small disorder optimal transport occurs only at vanishing dephasing rates where the FWHM is almost zero indicating an unfavorable, narrow absorption lineshape. In the opposite limit of very large dephasing the spectrum is quite broad, but the diffusion rate is also negligible (see (8)), which is also not optimal. As a result, engineering a material with both favorable transport properties and a absorption profile requires a delicate balance of the disorder and dephasing.

4. Applications

The dephasing rate in the HSR model may be obtained from a microscopic description of the environment that is characterized by a thermal bath of harmonic oscillators. By taking the high temperature limit of the bath correlation function one obtains the simple relationship, $\Gamma = 2k_b T \lambda / \omega_d$, where λ is the reorganization energy, ω_d is the associated Debye frequency of the material, and T is the temperature [43, 48, 49, 36]. Substituting this expression into (15) leads to a relationship for the temperature that maximizes the diffusion coefficient,

$$k_b T_{\max} \propto \frac{J \omega_d}{2 \lambda \xi}. \quad (20)$$

While a non-monotonic temperature dependence of the transport properties has indeed been observed experimentally in several molecular crystal thin films such as rubrene

and perylene [1, 2], a more accurate treatment of the thermal environment is required in order to conclusively confirm this interesting observation. Preliminary numerical calculations for a disordered system weakly coupled to a quantum harmonic bath have demonstrated that the diffusion constant does indeed exhibit a maximum as a function of temperature as predicted here [50]. However, the prediction of (20) has been shown to be only qualitatively correct.

In addition to the non-monotonic temperature dependence of the transport properties, recent experiments on the effect of disorder on the conductivity of the conducting polymer, polyaniline, also clearly illustrate the principles outlined in this work [51]. With conventional processing techniques, samples of polyaniline are highly disordered. This is manifested in experimental measurements by the appearance of a minimum in the resistivity as a function of temperature, and at temperatures below this point the resistivity increases rapidly due to disorder-induced localization. Through improved sample processing methods however, Lee et al. were able to reduce the amount of disorder present in polyaniline [51]. They demonstrated that the resistivity decreases uniformly as the sample quality improves, and additionally, the location of the minimum shifts to lower temperatures. This behavior is consistent with that seen in figure 2(a). By reducing the amount of disorder even further, the resistivity minimum disappears completely which has been interpreted as the onset of metallic behavior in polyaniline [51].

Finally as a simple predictive example, one may estimate the temperature at which the transport is maximized in arrays of the natural light harvesting system, LH2 [52]. A one-dimensional array of these photosynthetic complexes is relatively well characterized by the parameters, $\lambda = \sigma = 200 \text{ cm}^{-1}$, $\omega_d = 50 \text{ cm}^{-1}$, and an inter-ring coupling of $J = 50 \text{ cm}^{-1}$. With these values, (20) predicts a peak in the transport at $k_b T \approx 25 \text{ cm}^{-1}$. However, as mentioned above, in order to provide a definitive estimate, it will be essential to develop a more accurate description of the environment beyond the HSR model.

5. Conclusions

In conclusion, we have provided exact numerical results for the transport properties of infinite one-dimensional disordered systems coupled to a classical thermal environment. The limiting behavior at weak and strong dephasing, elucidated through the development of master equations in the respective limits, imply the existence of a maximal diffusion rate at intermediate dephasing. This prediction and the respective scaling relations have been confirmed numerically. While the results have been obtained within the HSR model, the scaling relations are generic and their generalization to systems described by a more realistic environment should be possible. Additionally we have shown that in the weak dephasing limit, the coherent quantum transport leads to diffusion rates that are much larger than would be predicted classically with an enhancement factor that is proportional to the localization length. The numerical results

presented in section 3.2 on the dynamical properties of the transport demonstrate that the MSD in the weak-dephasing regime may be described as a sum of the short-time, free particle motion in the Anderson localized chain and the long-time linear diffusion. The former behavior appears as a significant non-Gaussian contribution during the evolution of the probability distributions of the site populations. Finally the influence of the noise and disorder on the spectral lineshapes and the relation between the absorption spectrum and the optimal transport regime have been presented in the context of organic photovoltaic materials. While decreasing the amount of disorder improves the transport properties, it also leads to an undesirable narrowing of the absorption spectra. The need for both a broad spectrum and favorable transport characteristics requires a delicate balance of the disorder and dephasing.

The work presented here lays the foundation for a series of forthcoming results. As mentioned briefly in section 4, the extension of the HSR environment to a quantum environment is currently being explored through the use of recently developed non-Markovian stochastic Schrödinger equations [53]. Preliminary results display finite zero-temperature transport as well as an optimal diffusion rate as a function of temperature [50]. An additional topic of current focus is extending the model to higher dimensions and using more realistic non-nearest neighbor interactions to describe the electronic couplings. As has been recently reported, disordered systems with long-range interactions can develop a mobility edge and undergo an Anderson transition [54]. This has a profound impact on the transport properties and absorption characteristics. Finally, we are also exploring an extension of the HSR model in which the classical environment is modified to include non-Markovian effects describing the coupling of the system to under-damped vibrations. Both the relaxation time of the bath as well as the frequency of the vibrational modes have been seen to have an important influence on the transport properties. These interesting preliminary results are topics of ongoing work.

6. Acknowledgments

This work was supported by the NSF (Grant No. CHE-1112825) and DARPA (Grant No. N99001-10-1-4063). J. Moix and M. Khasin are supported by the Center for Excitonics, an Energy Frontier Research Center funded by the US Department of Energy, Office of Science, Office of Basic Energy Sciences under Award No. DE-SC0001088. J. Moix acknowledges a generous allocation of computing time from the Extreme Science and Engineering Discovery Environment (XSEDE), which is supported by the NSF (Grant No. OCI-1053575).

Appendix A. Absorption Spectrum

Herein exact expressions for the absorption spectrum in the presence of dephasing and disorder are presented [55]. In the absence of the bath, the absorption spectra is given

by Fermi's Golden Rule [47],

$$A(\omega) = \frac{1}{N} \sum_{\kappa} |\mu_{\kappa}|^2 \delta(\omega - \omega_{\kappa}) , \quad (\text{A.1})$$

where the dipole moments are given by

$$\mu_{\kappa} = \mu_0 \sum_n \langle \kappa | n \rangle . \quad (\text{A.2})$$

As before, Greek indices denote the basis of eigenstates of H_s with the corresponding eigenvalues, ω_{κ} . Henceforth, we assume that all of the molecules in the system are identical and possess the same dipole moment, $\mu_0 = 1$.

In the presence of the environment the absorption spectra is more conveniently obtained in the time domain from the dipole autocorrelation function (cf. (6)),

$$\langle \mu(t) \mu(0) \rangle = \text{Tr} [\mu e^{-iLt} \mu \rho_g] , \quad (\text{A.3})$$

where $\rho_g = |0\rangle\langle 0|$ is the ground state density matrix, and L is the Liouville operator for the total system and bath. Defining the initial state $\tilde{\rho} = \mu \rho_g$, its corresponding time evolution is given by the Liouville equation,

$$\dot{\tilde{\rho}} = -i [H_s, \tilde{\rho}] - \frac{\Gamma}{2} \sum_{n=1} [V_n, [V_n, \tilde{\rho}]] . \quad (\text{A.4})$$

Since the ground state is not coupled to the single excitation manifold or the bath, the equation of motion for the density matrix reduces to

$$\dot{\tilde{\rho}} = -i H_s \tilde{\rho} - \Gamma \tilde{\rho} . \quad (\text{A.5})$$

The same result may be obtained from the stochastic version of the HSR model either through the cumulant expansion or through the application of the Shapiro-Loginov formula [56]. Introducing the eigenstates of H_s and using $\mu|0\rangle = \mu_0 \sum_n |n\rangle$, the correlation function becomes,

$$\begin{aligned} \langle \mu(t) \mu(0) \rangle &= \sum_{\kappa} e^{-\Gamma t} e^{-i\omega_{\kappa} t} \langle \kappa | \mu | 0 \rangle \langle 0 | \mu | \kappa \rangle \\ &= e^{-\Gamma t} \sum_{\kappa} |\mu_{\kappa}|^2 e^{-i\omega_{\kappa} t} \end{aligned} \quad (\text{A.6})$$

If $\Gamma = 0$, then the Fourier transform of the dipole-dipole correlation function clearly leads back to (A.1). At finite dephasing one obtains the result,

$$A(\omega) \propto \sum_{\kappa} |\mu_{\kappa}|^2 \frac{\Gamma}{\Gamma^2 + (\omega - \omega_{\kappa})^2} , \quad (\text{A.7})$$

which illustrates that the presence of dephasing simply broadens each line in the dephasing-free spectrum into a Lorentzian of width Γ .

At very large disorder, $\sigma/J \gg 1$, the eigenstates are localized in the site basis. In this case, the dipole moments are all identical with $\mu_k = \mu_0$ which leads to a Gaussian spectrum in the zero dephasing limit. As the dephasing increases the spectrum becomes a convolution of a Gaussian with a Lorentzian – a Voigt profile. In the alternative limit of very large dephasing, the absorption spectrum becomes independent of the disorder,

as was also observed for the diffusion coefficients, and the lineshape acquires a purely Lorentzian profile with a half maximum that scales linearly with the dephasing rate as seen in figure 7(b).

References

- [1] Karl N, Kraft K, Marktanner J, Münch M, Schatz F, Stehle R and Uhde H 1999 *J. Vac. Sci. Technol. A* **17** 2318–2328
- [2] Podzorov V, Menard E, Borissov A, Kiryukhin V, Rogers J A and Gershenson M E 2004 *Phys. Rev. Lett.* **93** 086602
- [3] Sakanoue T and Sirringhaus H 2010 *Nature Materials* **9** 736–740
- [4] Akselrod G M, Tischler Y R, Young E R, Nocera D G and Bulovic V 2010 *Phys. Rev. B* **82** 113106
- [5] Dias F B, Kamtekar K T, Cazati T, Williams G, Bryce M R and Monkman A P 2009 *ChemPhysChem* **10** 2096–2104
- [6] Singh J, Bittner E R, Beljonne D and Scholes G D 2009 *J. Chem. Phys.* **131** 194905–194905–10
- [7] Dykstra T E, Hennebicq E, Beljonne D, Gierschner J, Claudio G, Bittner E R, Knoester J and Scholes G D 2008 *J. Phys. Chem. B* **113** 656–667
- [8] Bednarz M, Malyshev V A and Knoester J 2003 *Phys. Rev. Lett.* **91** 217401
- [9] Moix J, Wu J, Huo P, Coker D and Cao J 2011 *J. Phys. Chem. Lett.* **2** 3045–3052
- [10] Schofield S A and Wolynes P G 1995 *J. Phys. Chem.* **99** 2753–2763
- [11] Leitner D M and Wolynes P G 1996 *Phys. Rev. Lett.* **76** 216–219
- [12] Leitner D 2010 *New J. Phys.* **12** 085004
- [13] Goj A and Bittner E R 2011 *J. Chem. Phys.* **134** 205103–205103–11
- [14] Cho M, Vaswani H M, Brixner T, Stenger J and Fleming G R 2005 *J. Phys. Chem. B* **109** 10542–10556
- [15] Anderson P W 1958 *Phys. Rev.* **109** 1492
- [16] Ishii K 1973 *Prog. Theor. Phys. Supp.* **53** 77–138
- [17] Phillips P 1993 *Annu. Rev. Phys. Chem.* **44** 115–144
- [18] Kramer B and MacKinnon A 1993 *Rep. Prog. Phys.* **56** 1469–1564
- [19] Ingold G, Wobst A, Aulbach C and Hänggi P 2004 What do phase space methods tell us about disordered quantum systems? *Anderson Localization and Its Ramifications* vol 630 ed Brandes T and Kettemann S (Springer Berlin / Heidelberg) pp 85–97
- [20] Ping S 2006 *Introduction to Wave Scattering, Localization and Mesoscopic Phenomena* vol 88 (Springer)
- [21] Kenkre V M and Reineker P 1982 *Exciton Dynamics in Molecular Crystals and Aggregates* vol 94 (Springer)
- [22] Madhukar A and Post W 1977 *Phys. Rev. Lett.* **39** 1424–1427
- [23] Bulatov A, Kuklov A and Birman J L 1998 *Chem. Phys. Lett.* **289** 261–266
- [24] Amir A, Lahini Y and Perets H B 2009 *Phys. Rev. E* **79** 050105
- [25] Izrailev F M, Kottos T, Politi A and Tsironis G P 1997 *Phys. Rev. E* **55** 4951–4963
- [26] Thouless D J and Kirkpatrick S 1981 *Journal of Physics C: Solid State Physics* **14** 235–245
- [27] Mott N F 1969 *Philosophical Magazine* **19** 835–852
- [28] Logan D E and Wolynes P G 1987 *Phys. Rev. B* **36** 4135–4147
- [29] Mukamel S 1989 *Phys. Rev. B* **40** 9945–9947
- [30] Loring R F, Franchi D S and Mukamel S 1988 *Phys. Rev. B* **37** 1874–1883
- [31] Evensky D A, Scalettar R T and Wolynes P G 1990 *J. Phys. Chem* **94** 1149–1154
- [32] Yamada H and Ikeda K S 1999 *Phys. Rev. E* **59** 5214–5230
- [33] Cao J and Silbey R J 2009 *J. Phys. Chem. A* **113** 13825–13838
- [34] Hoyer S, Sarovar M and Whaley K B 2010 *New J. Phys.* **12** 065041
- [35] Miller A and Abrahams E 1960 *Phys. Rev.* **120** 745–755

- [36] Lloyd S, Mohseni M, Shabani A and Rabitz H 2011 *arXiv:1111.4982*
- [37] Wu J, Cao J and Silbey R J 2013 *Phys. Rev. Lett.*, *in press*
- [38] Wu J, Liu F, Ma J, Silbey R J and Cao J 2012 *J. Chem. Phys.* **137** 174111–174111–12
- [39] Ciuchi S, Fratini S and Mayou D 2011 *Phys. Rev. B* **83** 081202
- [40] Lee P A and Ramakrishnan T V 1985 *Reviews of Modern Physics* **57** 287–337
- [41] Mukamel S 1999 *Principles of Nonlinear Optical Spectroscopy* (Oxford University Press, USA)
- [42] Witkoskie J B, Yang S and Cao J 2002 *Phys. Rev. E* **66** 051111
- [43] Jayannavar A M and Kumar N 1988 *Phys. Rev. B* **37** 573–576
- [44] Moix J M, Zhao Y and Cao J 2012 *Phys. Rev. B* **85** 115412
- [45] de Laissardiere G T, Julien J and Mayou D 2006 *Phys. Rev. Lett.* **97** 026601
- [46] Klafter J and Jortner J 1978 *J. Chem. Phys.* **68** 1513–1522
- [47] Fidler H, Knoester J and Wiersma D A 1991 *J. Chem. Phys.* **95** 7880–7890
- [48] Wu J, Liu F, Shen Y, Cao J and Silbey R J 2010 *New J. Phys.* **12** 105012
- [49] Valteau S, Saikin S K, Yung M and Guzik A A 2012 *J. Chem. Phys.* **137** 034109–034109–13
- [50] Zhong X, Zhao Y and Cao J unpublished results
- [51] Lee K, Cho S, Park S H, Heeger A J, Lee C and Lee S 2006 *Nature* **441** 65–68
- [52] Escalante M, Lenferink A, Zhao Y, Tas N, Huskens J, Hunter C N, Subramaniam V and Otto C 2010 *Nano Letters* **10** 1450–1457
- [53] Zhong X and Zhao Y 2013 *J. Chem. Phys.* **138** 014111–014111–9
- [54] Rodríguez A, Malyshev V A, Sierra G, Martn-Delgado M A, Rodríguez-Laguna J and Domnguez-Adame F 2003 *Phys. Rev. Lett.* **90** 027404
- [55] Mukamel S 1985 *J. Chem. Phys.* **82** 5398–5408
- [56] Shapiro V E and Loginov V M 1978 *Physica A* **91** 563–574